World Academy of Science, Engineering and Technology
International Journal of Medical and Health Sciences
Vol:12, No:6, 2018

FZP Design Considering Spherical Wave Incidence

Sergio Pérez-López, Daniel Tarrazó-Serrano, José M. Fuster, Pilar Candelas, Constanza Rubio

***Abstract*—**Fresnel Zone Plates (FZPs) are widely used in many areas, such as optics, microwaves or acoustics. On the design of FZPs, plane wave incidence is typically considered, but that is not usually the case in ultrasounds, especially in applications where a piston emitter is placed at a certain distance from the lens. In these cases, having control of the focal distance is very important, and with the usual Fresnel equation a focal displacement from the theoretical distance is observed due to the plane wave supposition. In this work, a comparison between FZP with plane wave incidence design and FZP with point source design in the case of piston emitter is presented. Influence of the main parameters of the piston in the final focalization profile has been studied. Numerical models and experimental results are shown, and they prove that when spherical wave incidence is considered for the piston case, it is possible to have a fine control of the focal distance in comparison with the classical design method.

***Keywords*—**Focusing, Fresnel zone plate, ultrasound, spherical wave incidence, piston emitter.

I. Introduction

ZONE PLATES (ZPs) are used for wave focusing applications in situations where planar fabrication is easier or more advantageous over conventional curved lenses. Recently, new types of ZPs have been presented, such as Fractal ZPs based on binary cantor sequences [1]-[3], which present multiple foci that help to reduce chromatic aberration; or M-bonacci ZPs [4], [5], which result in bifocal focusing profiles with equal intensity in both foci. Among the different types of ZPs, FZPs are the most common type for single focus applications and they are used in many areas of physics, such as optics [6], [7], microwaves [8], [9] or acoustics [10], [11].

Conventional FZPs focus due to constructive interference of the diffracted fields. They consist of a set of concentric rings, each one them being a Fresnel region. Depending on the implementation of the different regions FZPs can be classified into two types. Soret FZPs [12] alternate blocking zones with transparent zones, while Rayleigh-Wood FZPs [13] replace blocking zones with phase reversal zones.

One important application of wave focusing devices in ultrasound domain is tumour ablation through High Intensity Focused Ultrasound (HIFU) [14]. In this context, having a fine control of the focal distance is very important, and the incident wavefront type has to be considered in order to avoid distortion in the FZP focusing profile. In HIFU, underwater transducers are used because of the better sound propagation characteristics of water in comparison with air. Moreover, the characteristic impedance of the water is similar to the human body impedance, which reduces the impedance mismatch and increases the energy efficiency of the treatment. Piston emitters are the most common transducer type for underwater applications, and therefore their influence in the FZP focusing profile has to be studied.

This work presents a comparison between plane wave and spherical wave incidence, as well as a study of the piston emitter main parameters and their influence on the FZP focusing properties.

Sergio Pérez-López, Daniel Tarrazó-Serrano, and Pilar Candelas are with Centro de Tecnologías Físicas, Universitat Politècnica de València, Camí de Vera s/n, 46022, València, Spain (e-mail: serpelo1@upv.es, dtarrazo@fis.upv.es, pcandelas@fis.upv.es).

José M. Fuster is with Departamento de Comunicaciones, Universitat Politècnica de València, Camí de Vera s/n 46022, València, Spain (e-mail: jfuster@dcom.upv.es).

Constanza Rubio is with Centro de Tecnologías Físicas, Universitat Politècnica de València, Camí de Vera s/n, 46022, València, Spain (Corresponding author; e-mail: crubiom@fis.upv.es).

II. Influence of Incident Wavefront

As mentioned before, the type of incident wavefront on the FZP has to be considered in order to have a good control of the focal distance.

The focusing profile of the FZP, independently of the incident wavefront, can be numerically calculated using the Fresnel diffraction integral [15]:

$$p(z) = \frac{2\pi}{j\lambda}\int_0^{r_N} p_i(r) r \frac{e^{jkR}}{R} dr, \quad (1)$$

where r_N is the maximum radius of the FZP, $p_i(r)$ is the incident pressure at the FZP aperture, r is the radial coordinate at the FZP plane, $\mathrm{k} = 2\pi/\lambda$ is the propagation constant with λ being the working wavelength, and $R = \sqrt{r^2 + z^2}$, being z the axial coordinate.

A. Plane Wave Incidence

For plane wave incidence, the incident pressure at the FZP would be:

$$p_i = p_0 e^{j\theta_0}, \quad (2)$$

where p_0 is an amplitude constant and θ_0 is a phase constant.

The radii of the different Fresnel regions of the FZP can be calculated by assuming a π phase difference of the pressure produced by two consecutive radii at the focal distance, which results in a difference of $\lambda/2$ in the pressure propagation paths from the radius itself to the focal distance. In a Soret type FZP, transparent zones produce that only in-phase contributions interfere at the focal distance, while the destructive interference with π phase difference with the contributions of the transparent zones is blocked at the blocking zones. Thus, the Fresnel radii equation for plane wave incidence is given by

$$F + \frac{n\lambda}{2} = \sqrt{F^2 + r_n^2}, \quad (3)$$

where F is the focal distance, r_n is the n-th Fresnel radius and $n = 1, 2, \ldots, N$, being N the total number of Fresnel radii.

Once the focal distance and the frequency is fixed, the only design parameter is N. Fig. 1 shows the normalized axial intensity for a FZP designed with (3) for a focal distance of $F = 15\lambda$ and different number of Fresnel radii. As it can be observed, as N increases, the Full Length Half Maximum (FLHM) is reduced and the intensity at the focal distance increases.

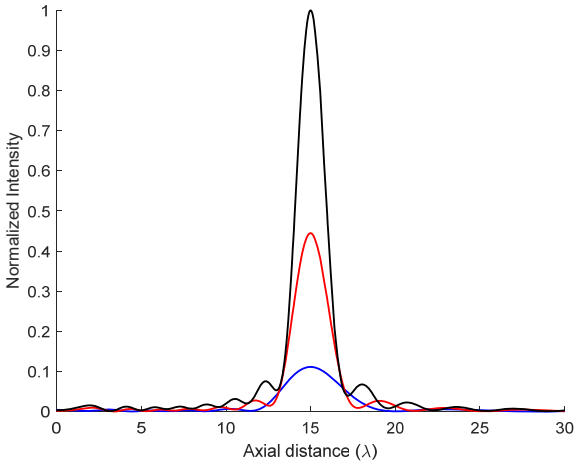

Fig. 1 Normalized axial intensity for different N values: $N = 11$ for blue solid line, $N = 21$ for red solid line and $N = 31$ for black solid line

B. Spherical Wave Incidence

In many areas of physics, such as microwave or optics, plane wave incidence is typically supposed, but in ultrasound domain, the distance between the emitter and the FZP is usually not enough to consider plane wave [11]. In this case, the incident pressure on the FZP would be given by

$$p_i(r) = \frac{p_0}{R} e^{-jkR}, \quad (4)$$

where $R = \sqrt{d^2 + r^2}$, being d the distance between the point source emitter and the FZP.

The condition for constructive interference is the same as for plane wave incidence: the difference between pressure propagation paths of two consecutive radii has to be $\lambda/2$. Therefore, the Fresnel radii for spherical wave incidence can be calculated using the following equation:

$$d + F + \frac{n\lambda}{2} = \sqrt{d^2 + r_n^2} + \sqrt{F^2 + r_n^2} \quad (5)$$

If (5) is used to design the FZP for the spherical wave incidence situation, the resulting focusing profile is the same as shown in Fig. 1. However, it is interesting to study the distortion introduced in the focusing profile when there is spherical wave incidence but the FZP has been designed with (3). Hence, the phase error introduced if it is considered a constant phase of the incident wavefront but there is a point source placed at a distance d from the FZP is given by:

$$\phi_e = k(\sqrt{d^2 + r^2} - d). \quad (6)$$

Fig. 2 shows the phase error of the incident wavefront for different emitter distances as a function of the radial coordinate of the FZP. As it can be seen, the closer the source emitter is, the bigger the phase error. Therefore, if the emitter distance is not enough, some distortion must be expected in the focusing profile of the FZP, since the phase difference between the propagation paths of two consecutive radii is no longer π and the constructive interference condition at the focal distance is not valid.

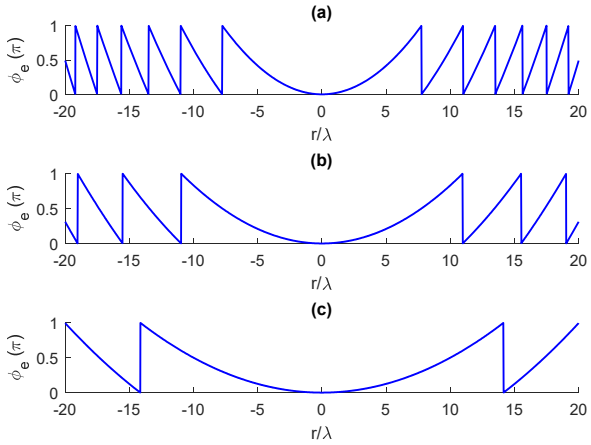

Fig. 2 Phase error for different d values: (a) $d = 60\lambda$, (b) $d = 120\lambda$ and (c) $d = 200\lambda$

In order to evaluate the distortion, the focal displacement (ΔF) and the increase in the FLHM value ($\Delta FLHM$) have been calculated for three FZP with the same number of Fresnel radii ($N = 21$) but different focal distances. Fig. 3 shows the results of a FZP with $F = 15\lambda$ (blue line), a FZP with $F = 25\lambda$ (red line) and a FZP with $F = 35\lambda$ (black line). As it can be observed from Fig. 3 (a), as the distance from point source to the FZP is reduced, the focal displacement increases for the three FZP. Moreover, the focal shift is bigger as the focal distance of the FZP increases. This phenomenon is due to the increase in the FZP size as the focal distance augments, resulting in a bigger phase error of the incident wavefront. Fig. 3 (b) shows the FLHM increase referred to the ideal value obtained for plane wave incidence, and it can be observed that the reduction of the distance between the source and the FZP results in a significantly wider focus.

Distortion in the focusing profile not only results in a focal displacement from its theoretical focal distance and a wider focus, but it results in a reduction of the maximum intensity too. Fig. 4 depicts the numerically computed axial intensities for one FZP with $N = 21$ and $F = 15\lambda$, with three different point source emitter distances. As it can be seen, as d increases the focal distance is closer to its theoretical value and the FLHM is reduced.

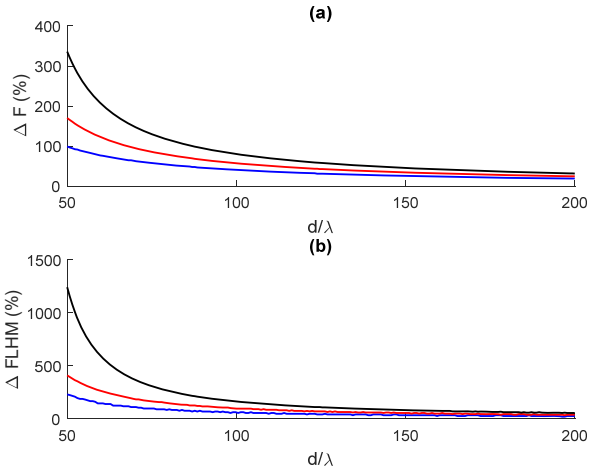

Fig. 3 (a) Focal displacement and (b) $\Delta FLHM$ as a function of d for different focal distances: $F = 15\lambda$ for blue solid line, $F = 25\lambda$ for red solid line and $F = 35\lambda$ for black solid line

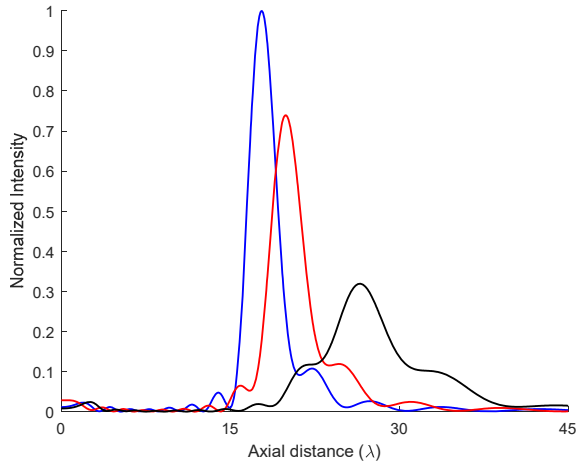

Fig. 4 Normalized axial intensity for different d values: $d = 200\lambda$ for blue solid line, $d = 120\lambda$ for red solid line and $d = 60\lambda$ for black solid line

III. Piston Emitter

A piston emitter is a circular shape piezoelectric transducer that is widely employed in ultrasound applications. Ideally, the piston surface moves with uniform speed, which generates a pressure field that can be analytically calculated for two different situations: near field or Fresnel region, and far field or Fraunhofer region [15]. In the Fresnel region, the pressure field is highly variable in phase and amplitude, and this is not a desirable behaviour for the incident wavefront on the FZP. Therefore, it is desirable that the piston works in the far field, where the pressure is proportional to R^{-1}. The far field or Fraunhofer distance is given by

$$z > \frac{2D^2}{\lambda}, \tag{7}$$

where $D = 2a$ is the piston source active diameter, being a the piston radius. As a function of the ka product value, the distance is

$$\frac{z}{\lambda} > \frac{2}{\pi^2}(ka)^2. \tag{8}$$

Thus, in the Fraunhofer region a piston emitter can be modelled as a point source with a specific directivity pattern $D(\theta)$:

$$p_i(r,\theta) \propto \frac{1}{R} D(\theta) e^{-jkR}, \tag{9}$$

where $R = \sqrt{d^2 + r^2}$, being d the distance from the piston to the FZP; and $D(\theta)$ is given by

$$D(\theta) = \frac{2J_1(ka \sin\theta)}{ka \sin\theta}, \tag{10}$$

being θ the angle referred to the normal direction of the piston surface and J_1 the first kind and first order Bessel function.

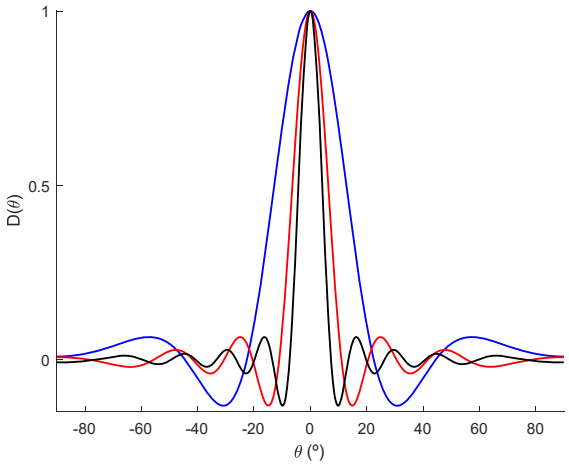

Fig. 5 $D(\theta)$ for different ka values: $ka = 10$ for blue solid line, $ka = 20$ for red solid line and $ka = 30$ for black solid line

The piston directivity pattern is a measure of how the piston spatially distributes the energy as a result of the destructive and constructive interferences generated by the piston surface. Fig. 5 shows the piston directivity pattern for different ka values. As it can be observed, as the ka product increases the piston becomes more directional, which would result in a worse behavior of the FZP because the pressure field incident on the lens differs substantially from the ideal point source case. Increasing the ka value can be understood as increasing the piston active radius at a given frequency, or increasing the working frequency for a specific piston radius. Hence, the piston influence in the FZP focusing profile is determined by its directivity pattern. There are two main parameters that contribute to the distortion of the focusing profile: the amplitude of $D(\theta)$ and its phase. The amplitude influence cannot be corrected as it would require some gain mechanism at the FZP to compensate the variation of the incident wavefront amplitude with θ. The π-phase change between two consecutive secondary lobes of $D(\theta)$ will produce that some of the outer Fresnel regions of the FZP interfere destructively at the focal distance. Fig. 6 depicts the normalized axial intensity of a FZP designed for spherical wave incidence for

different ka values of a piston placed at $d = 100\lambda$. As it can be observed, when $ka = 10$ (blue solid line) the piston influence in the focusing profile is not noticeable, whereas for the $ka = 20$ situation (red solid line) severe amplitude distortion is present, with a decrease in the intensity level at the focal distance and an increase in the FLHM value. For the $ka = 30$ case (black solid line), the π-phase change of the incident wavefront introduced by the secondary lobes results in destructive interference at the theoretical focal distance. Thus, the distortion in the focusing profile increases with the piston directivity. Nevertheless, it is worth noting that the piston does not introduce a focal displacement from the theoretical focal distance as long as there is no significant phase error from $D(\theta)$ secondary lobes.

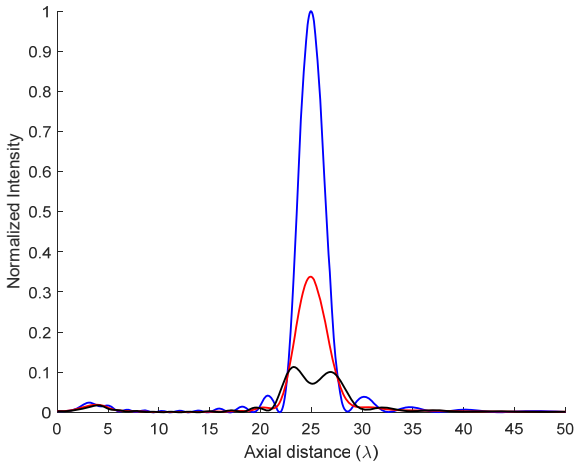

Fig. 6 Simulations for a FZP designed with spherical wave incidence consideration for different ka values: $ka = 10$ for blue solid line, $ka = 20$ for red solid line and $ka = 30$ for black solid line

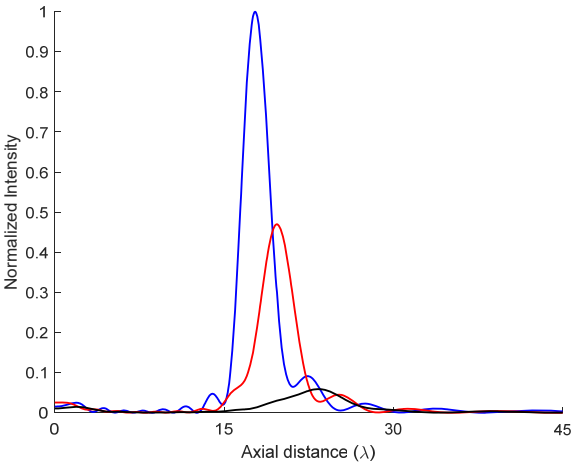

Fig. 7 Simulations for plane wave FZP design and piston emitter with $ka = 15$: $d = 200\lambda$ for blue solid line, $d = 120\lambda$ for red solid line and $d = 60\lambda$ for black solid line

It is also interesting to study the distortion of the focusing profile when there is a piston emitter but plane wave incidence has been considered for the FZP design. Fig. 7 shows the normalized axial intensity for the same FZP of Fig. 4, but considering a piston emitter with $ka = 15$ instead of an ideal point source. Similar results are observed in terms of focal displacement. However, for the piston case focal intensity is decreased faster than for the point source case as source and the FZP become closer; and it is a consequence of the amplitude distortion introduced by $D(\theta)$.

IV. Experimental Results

In order to prove the validity of the simulation results, experimental measurements have been carried out. A needle hydrophone form Precision Acoustics Ltd. with 1.5 mm of diameter is used as receiver, while a piston transducer with 32 mm of active diameter from Inmasonic is used as transmitter. The input signal of the piston is generated using a Panametrics 5077PR Pulser and the received signal at the hydrophone is digitized using a digital oscilloscope from Pico Technology with a resolution of 12 bits. An underwater 3D automated positioning system with a spatial resolution of $1 \times 1 \times 1$ mm^3 is used to control the measure points inside a water tank.

There have been manufactured two Soret FZP made of brass for the experimental measurements. Both have $N = 27$ Fresnel radii and a focal distance of $F = 50$ mm for a working frequency $f_0 = 250$ kHz, but one of them is designed with plane wave consideration and other with spherical wave consideration for a source separation distance of $d = 350$ mm. The underwater sound speed is $c_w = 1500$ m/s. Fig. 8 shows the two FZP, being Fig. 8 (a) the plane wave design and Fig. 8 (b) the spherical wave design.

Fig. 9 shows the measured intensity maps normalized to the maximum. As it can be observed from the comparison between Figs. 9 (a) and (b), the FZP designed with plane wave consideration shows a focal displacement from its theoretical focal distance, whereas the FZP designed in the assumption of spherical wave achieves its theoretical focal distance of 50 mm and produces a narrower focus with higher intensity.

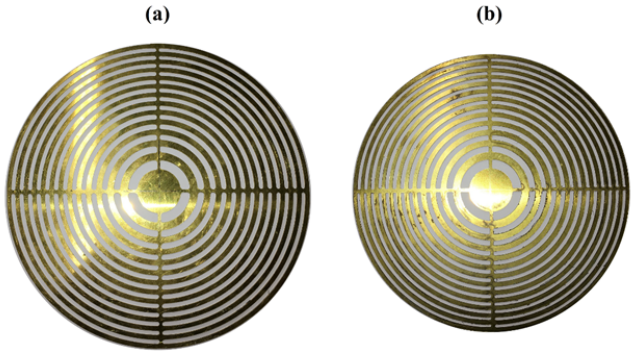

Fig. 8 (a) FZP designed for plane wave incidence and (b) FZP designed for spherical wave incidence

Fig. 10 shows the measured focusing profiles along the axial distance for both FZP. Blue and red lines correspond to the FZP with plane wave design and the FZP designed for spherical wave incidence, respectively. Dashed lines represent the FZP numerically computed axial intensities using (1), whereas solid lines represent the experimental results,

showing a good agreement between them. As it can be seen, the FZP with plane wave design shows a focal displacement $\Delta F = 40\%$ compared to its theoretical position and it presents a reduction in the intensity level of 30%. FZP with spherical wave design shows a FLHM of 15 mm, while the plane wave design shows a FLHM of 21 mm, which represent an increase of $\Delta FLHM = 50\%$ and $\Delta FLHM = 110\%$ over the ideal case ($FLHM_0 = 10$ mm), respectively. For the FZP with spherical wave design, the FLHM increase is mainly due to the piston amplitude distortion, whereas for the FZP with plane wave design the increase is mainly due to the incident wavefront phase error.

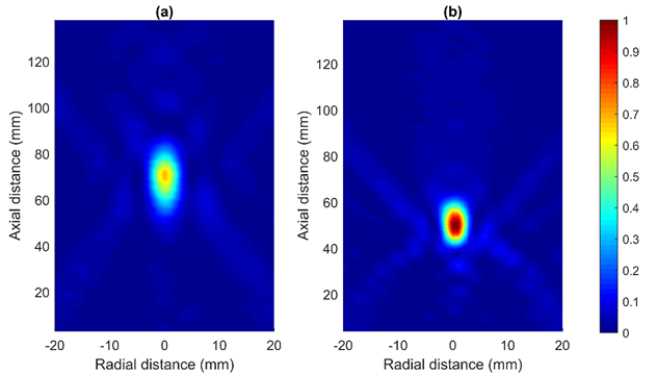

Fig. 9 Measured normalized intensity maps: (a) FZP design for plane wave incidence and (b) FZP design for spherical wave incidence

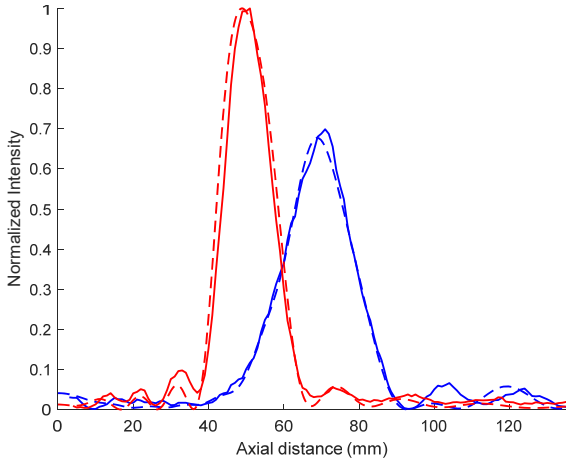

Fig. 10 Measured intensity focusing profiles: FZP design with plane wave simulation (blue dashed line) and results (blue solid line); and FZP design with spherical wave simulation (red dashed line) and results (red solid line)

V. Conclusion

In this work, it has been analysed the effect of the incident wavefront type on the FZP focusing profile. The error arising from designing a FZP for plane wave incidence when there is spherical wave incidence has been analysed through simulations, showing a focal displacement and an increase in the FLHM. The influence of the piston transducer has been analysed, and experimental measurements have been presented, showing a good agreement with simulation results.

Acknowledgment

This work has been supported by TEC2015-70939-R (MINECO/FEDER).

References

[1] A. Calatayud, V. Ferrando, F. Giménez, W. D. Furlan, G. Saavedra, and J. A. Monsoriu, "Fractal square zone plates," Opt. Commun., vol. 286, no. 1, pp. 42–45, Jan. 2013.
[2] O. Mendoza-Yero, M. Fernández-Alonso, G. Mínguez-Vega, J. Lancis, V. Climent, and J. A. Monsoriu, "Fractal generalized zone plates," J. Opt. Soc. Am. A, vol. 26, no. 5, p. 1161, 2009.
[3] G. Saavedra, W. D. Furlan, and J. A. Monsoriu, "Fractal zone plates," Opt. Lett., vol. 28, no. 12, p. 971, 2003.
[4] F. Machado, V. Ferrando, W. D. Furlan, and J. A. Monsoriu, "Diffractive m-bonacci lenses," Opt. Express, vol. 25, no. 7, p. 8267, Apr. 2017.
[5] J. A. Monsoriu, A. Calatayud, L. Remon, W. D. Furlan, G. Saavedra, and P. Andres, "Bifocal Fibonacci Diffractive Lenses," IEEE Photonics J., vol. 5, no. 3, pp. 3400106–3400106, Jun. 2013.
[6] I. Mohacsi et al., "Interlaced zone plate optics for hard X-ray imaging in the 10 nm range," Sci. Rep., vol. 7, p. 43624, Mar. 2017.
[7] O. Carnal, M. Sigel, T. Sleator, H. Takuma, and J. Mlynek, "Imaging and focusing of atoms by a fresnel zone plate," Phys. Rev. Lett., vol. 67, no. 23, pp. 3231–3234, Dec. 1991.
[8] S. M. Stout-Grandy, A. Petosa, I. V. Minin, O. V. Minin, and J. S. Wight, "Novel reflector-backed Fresnel zone plate antenna," Microw. Opt. Technol. Lett., vol. 49, no. 12, pp. 3096–3098, Dec. 2007.
[9] H. D. Hristov and M. H. A. J. Herben, "Millimeter-wave Fresnel-zone plate lens and antenna," IEEE Trans. Microw. Theory Tech., vol. 43, no. 12, pp. 2779–2785, 1995.
[10] D. C. Calvo, A. L. Thangawng, M. Nicholas, and C. N. Layman, "Thin Fresnel zone plate lenses for focusing underwater sound," Appl. Phys. Lett., vol. 107, no. 1, p. 014103, Jul. 2015.
[11] J. Fuster, P. Candelas, S. Castiñeira-Ibáñez, S. Pérez-López, and C. Rubio, "Analysis of Fresnel Zone Plates Focusing Dependence on Operating Frequency," Sensors, vol. 17, no. 12, p. 2809, Dec. 2017.
[12] J. L. Soret, "Ueber die durch Kreisgitter erzeugten Diffractionsphänomene," Ann. der Phys. und Chemie, vol. 232, no. 9, pp. 99–113, 1875.
[13] J. Kirz, "Phase zone plates for x rays and the extreme uv," J. Opt. Soc. Am., vol. 64, no. 3, p. 301, Mar. 1974.
[14] R. O. Illing et al., "The safety and feasibility of extracorporeal high-intensity focused ultrasound (HIFU) for the treatment of liver and kidney tumours in a Western population," Br. J. Cancer, vol. 93, no. 8, pp. 890–895, 2005.
[15] J. W. Goodman, Introduction to Fourier optics. Roberts and Company Publishers, 2005.